Reprogramming genetic circuits using space

Lorea Alejaldre[1†], Jesús Miró-Bueno[1†], Angeles Hueso-Gil[1], Lewis Grozinger[1], Huseyin Tas[2‡], Sina Geißler[1], and Ángel Goñi-Moreno[1*]

[1]Centro de Biotecnología y Genómica de Plantas, Universidad Politécnica de Madrid (UPM)-Instituto Nacional de Investigación y Tecnología Agraria y Alimentaria (INIA/CSIC), 28223, Madrid, Spain

[2]Systems Biology Department, Centro Nacional de Biotecnologia-CSIC, Campus de Cantoblanco, Madrid, 28049, Spain

[†]These authors contributed equally to this work.

[‡]Current affiliation: Department of Genetics, Harvard Medical School, 77 Avenue Louis Pasteur, Boston, MA 02115

[*]Address correspondence to: angel.goni@upm.es

Abstract

Genetic circuits confer computing abilities to living cells, performing novel transformations of input stimuli into output responses. These genetic circuits are routinely engineered for insertion into bacterial plasmids and chromosomes, using a design paradigm whose only spatial consideration is a linear ordering of the individual components. However, chromosomal DNA has a complex three dimensional conformation which alters the mechanics of gene expression, leading to dynamics that are specific to chromosomal location. Here we demonstrate that because of this, position in the bacterial chromosome is crucial to the function of synthetic genetic circuits, and that three dimensional space should not be overlooked in their design. Our results show that genetically identical circuits can be reprogrammed to produce different outputs by changing their spatial positioning and configuration. We engineer 221 spatially unique genetic circuits of four different types, three regulatory cascades and a toggle switch, by either inserting the entire circuit in a specific chromosomal position or separating and distributing circuit modules. Their analysis reveals that spatial positioning can be used not only to optimize circuits but also to switch circuits between modes of operation, giving rise to new functions. Alongside a comprehensive characterization of chromosomal space using single-cell RNA-seq profiles and Hi-C interaction maps, we offer baseline information for leveraging intracellular space as a design parameter in bioengineering.

1 Introduction

The design and implementation of genetic circuits for processing biological information is a central theme in synthetic biology [1, 2, 3]. In these circuits, genetic components receive input

signals, and output responses are generated based on instructions encoded into gene regulatory networks. This input-algorithm-output pipeline, aligning with the concept of computation [4], finds applications in various fields, such as bioproduction [5], pollution control [6] or medical diagnosis [7]. Different host organisms are used for this purpose, often chosen based on the specific application. For example, genetic circuits are now routinely engineered in bacteria [8], yeast [9], plants [10], or mammalian cells [11].

While the selection of DNA parts is crucial for circuit function, and testing libraries of parts is a common practice for fine-tuning circuit performance [12, 13], recent years have seen growing interest in the role played by their host context [14, 15, 16]. This refers to the cellular machinery surrounding and interacting with genetic circuits. As a result of these interactions, DNA parts may show different dynamics according to their context, leading to variations in circuit behaviour across different cellular hosts [17]. However, the context is typically considered a dimensionless parameter with no spatial implications. Yet, cells are three-dimensional entities, and even in bacteria (the smallest of them) molecular machineries are not homogeneously distributed throughout the entire cellular volume [18, 19]. Specifically, the chromosome occupies space, and genes are situated at given coordinates. For example, the location of certain genes close to the origin of replication (oriC) or co-localization of co-regulated genes has been proposed to provide a selective advantage for their expression and regulation [20, 21, 22]. Consequently, synthetic functions may require a specific address within the volume of the cell—an aspect deserving further attention and that underpins the present work. Ultimately, if evolution has shaped specific spatial configurations for the optimal performance of molecular systems, synthetic biology may find value in incorporating space as a design principle for engineering genetic circuits.

Spatial effects in eukaryotic cells are more extensively described compared to bacteria [23, 24, 25]. Intuitively, one might assume that the presence of physical compartments, higher DNA compaction, and larger volumes in eukaryotic cells makes spatial considerations more significant. However, it should not be assumed that space is not a significant factor in bacteria due to their smaller size [26]; indeed, it has been shown that not only are translation and transcription machineries heterogeneously distributed across the cytoplasm [27, 28, 29, 22], but also other types of resources such as enzymes or metabolites are allocated unequally [30]. Moreover, synthetic constructs have been shown to behave differently based on the specific genomic location where they are inserted, with the common practice being the random integration of the target gene(s) in the genome to select the best-performing position [31, 32, 33, 34], therefore using space for optimization.

The allocation of resources such as ribosomes or polymerases within bacterial cells, crucial for the functioning of synthetic constructs, has strong ties to how the chromosome is organized. For instance, genes relevant to generating these resources tend to be positioned in proximity to the oriC [35, 20]. This specific location confers the advantage of early duplication, resulting in a higher gene dosage throughout the cell lifecycle. Consequently, synthetic constructs located in this area would, in principle, have access to a more robust expression machinery [36, 37]. Other factors, such as DNA supercoiling, upstream transcription or extended protein

occupancy domains (EPODs) [38, 39], which are intrinsically space-dependent, can determine how genetic circuits perform depending on the insertion position. Moreover, circuits can be distributed across several locations, the physical separation between them being another spatial aspect with its own dynamics [40].

While successful strategies exist to insulate circuits from their genomic context [41], thus avoiding modulation effects depending on position, we argue that chromosomal dynamics [42] can be effectively harnessed and turned into design principles for a new wave of 3D circuits [43]. This becomes even more crucial as circuit complexity increases. Beyond optimizing the expression levels of a single gene, complex circuit behaviors would be intricately affected by spatial modulation. For instance, a basic spatial feature like gene orientation has been shown to play a more significant role in modulating the function of a toggle switch [44] than an expression system [36]. The question that arises is: can space be utilized not only to optimize but also to engineer new biological functions without altering the DNA sequences of synthetic constructs?

In this study, we employ the soil bacterium and synthetic biology chassis *Pseudomonas putida* KT2440 [45, 46, 47, 48] to address this question by analyzing a variety of genetic circuits. The results demonstrate that manipulating the spatial organization of circuits can expand their functionality. This expansion ranges from selecting the gene expression noise pattern of individual genes to transforming the functioning of a toggle switch into a sensor switch. Based on these findings, we contend that intracellular space can be effectively leveraged to design functions beyond mere sequences, paving the way for a whole-cell design approach in bioengineering.

2 Results and discussion

Generation of spatial genetic circuits

To investigate the influence of intracellular space in *Pseudomonas putida* KT2440 on circuit performance, we generated 221 genetic variants, each presenting a specific spatial configuration of a genetic construct. These circuits represent space-specific variants derived from four distinct initial constructs, including one toggle switch and three transcriptional cascades. Consequently, we introduced two distinct design features: the intrinsic properties of the genetic components and their spatial arrangement within the volume of the cell. By decoupling these two functional aspects, we illustrate the potential for controlling the spatial layer and its impact on circuit behaviour (Figure 1A). In other words, while the DNA sequence outlines a genetic program, the spatial layer empowers us to reprogram it in various ways. The objective of reprogramming complex phenotypes, such as the bistability exhibited by a toggle switch, is twofold: first, to assess the extent to which spatial positioning modulates them by quantifying all dynamics in between, leading to an optimisation strategy; and second, we aim to elucidate the emergence of new functions, enhancing the reusability of synthetic circuits for different tasks.

For transcriptional cascades, our reprogramming efforts aimed at achieving distinct expres-

sion noise profiles (Figure 1A), a crucial factor for the viability of larger circuits. These noise patterns capture the dynamic range of logic modules, ultimately influencing the compatibility of components within the circuit. Beyond their impact on biological computations, expression noise bears biological significance, such as its potential use in deploying beneficial phenotypes like bet-hedging or division of labour strategies. While conventional approaches achieved this by swapping DNA promoters or ribosome binding sites (RBSs), we achieved similar outcomes by altering the spatial location. To further characterize this effect, we constructed six different libraries of transcriptional cascades (Figure 1B). Four libraries utilized transcriptional repressors (libraries l with LacI and t with TetR), while two employed a transcriptional inducer (a with AraC). Three libraries were designed with all the genetic components inserted together at a specific chromosomal position (l_0, t_0, and a_0). The remaining three libraries were modularized into two distinct modules and independently distributed across the chromosome (l_m, t_m, and a_m). This separation was conducted such that one module, containing the transcriptional regulator, was consistently positioned at the *attTn7* site, while the other module, housing its cognate promoter and the reporter gene, was randomly inserted.

All performance variations resulting from distinct spatial arrangements were consistent across replicates and not the consequence of fluctuations or randomness (see Methods). This reinforces the significance of space as a design layer and indicates fundamental mechanistic differences based on location, essentially forming microenvironments within the intracellular space. To comprehensively characterize the chromosome of the host cell used in this study and its internal mechanistic details in terms of 3D space and 1D activity, we generated Hi-C interaction maps and contrasted with the transcriptional profile based on RNA-seq results, respectively.

The 3D space and 1D activity of *Pseudomonas putida* KT2440

While *P. putida* KT2440 serves as a widely-used chassis in synthetic biology and biotechnology, its intracellular spatial configuration has often been qualitatively or indirectly studied. We conducted quantitative experiments to evaluate the spatial impact of key mechanistic details crucial for the operation of our genetic circuits, specifically the physical interactions between chromosomal areas (3D space) and integrated the transcriptional profile of all positions (1D activity).

The Hi-C contact matrix in Figure 1C depicts the strength of pairwise interactions between chromosomal regions. Aside from featuring a typical diagonal line, indicating strong interactions within a region and its neighbors, this matrix reveals which areas of the chromosome exhibit stronger or weaker overall cumulative interactions—a parameter referred to as the *openness* of a location, encapsulating 3D spatial dynamics. For instance, the chromosomal region containing the *attTn7* site (of particular interest in this study, as half of the modules in m libraries are located there) and its interaction with every region yields the outer Hi-C interactions Tn7 ring in Figure 1D and the sum of all interactions in a specific region with all others except itself yields the inner HiC openness ring in Figure 1D. This figure offers a circular representation of KT2440 chromosome, emphasizing various results of our study. As observed

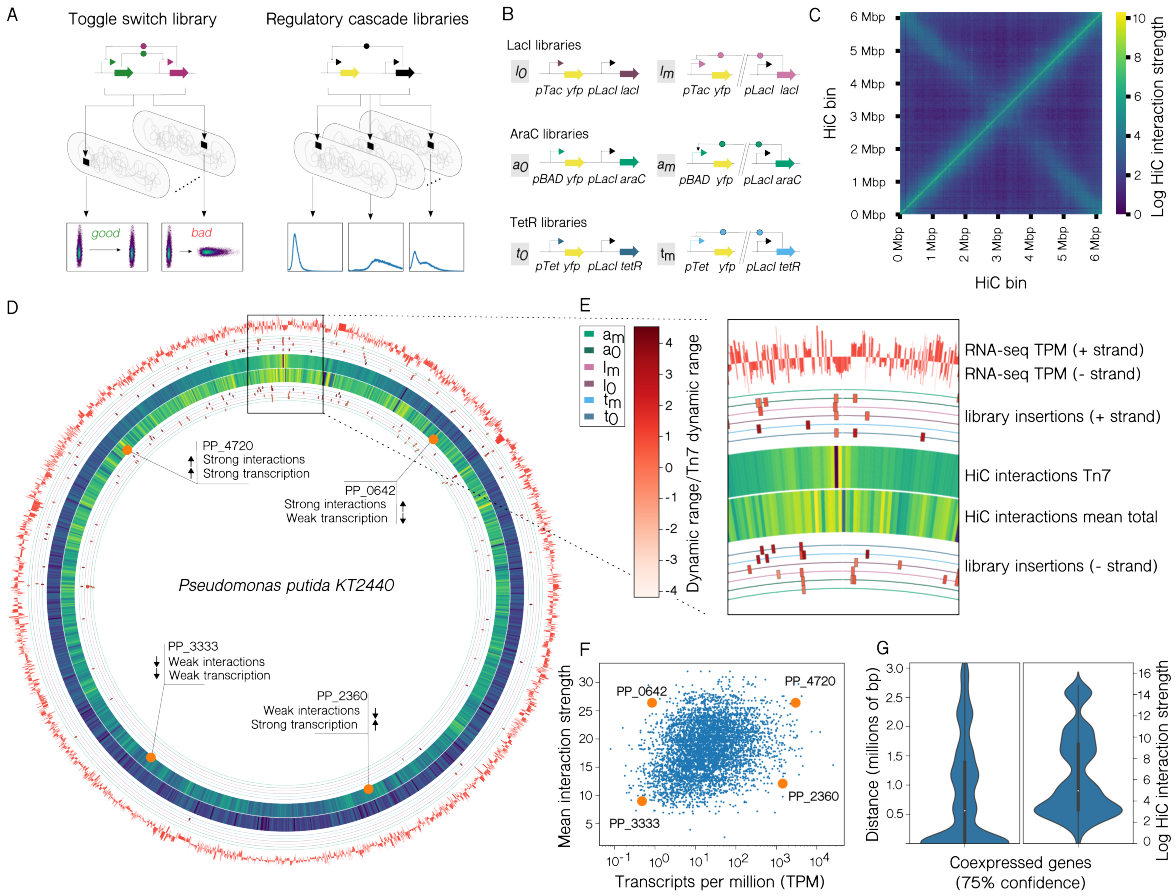

Figure 1: An overview of spatial genetic circuits inserted in a three dimensional *P. putida* chromosome. **A)** We insert two different types of circuit, toggle switches and regulatory cascades, into different chromosomal locations. The phenotype of genetically identical circuits can be reprogrammed by changing where they are inserted. **B)** The three different regulatory cascade circuits used, based on two repressors (LacI and TetR) and one inducer (AraC). For each circuit we tested libraries with all genetic components are placed together (l_0, t_0 and a_0), and with the circuit *modularised* and separately distributed across the chromosome (l_m, t_m and a_m). **C)** HiC contact matrix showing the strength of pairwise interactions between different regions of the *P. putida* KT2440 chromosome (a higher resolution version is included as Figure S1). **D)** HiC interactions alongside RNA-seq analysis of the entire chromosome. Locations where circuits are inserted are marked using a circle for each regulatory cascade library. Four positions are highlighted (orange circles), corresponding to loci with different interaction (HiC) and transcription (RNA-seq) strength (a higher resolution version is included as Figure S2). **E)** An enlarged section of the full-chromosome of panel D. The six regulatory cascade libraries are shown on coloured rings, with boxes marking their insertion position, and the colour of the box corresponding to the dynamic range of the circuit compared to that of the same circuit inserted at the Tn7 site. **F)** The transcripts per million (TPM) for each loci obtained from RNA-seq analysis is plotted against their mean HiC interaction with all other parts of the chromosome. Orange dots correspond to those highlighted in panel D. **G)** Pairs of coexpressed genes in *P. putida* KT2440, according to the STRING database. Plots show the distribution of the linear distance between them in base pairs (left) and the interaction strength between them as taken from the HiC contact matrix.

in the zoom-in segment (Figure 1E), interactions with the *attTn7* site are stronger in its vicinity and attenuate as we move farther away in the chromosome. Calculating the openness value for all regions (inner Hi-C circle) reveals substantial variation within the chromosome, even among proximal areas. In essence, certain regions tend to interact more extensively with others, and this characteristic is not uniformly distributed across the chromosome.

Understanding the genomic context through 1D activity, encompassing upstream and downstream transcription activity, is crucial for interpreting the performance of our libraries of inserted constructs. To evaluate the influence of this parameter, we used RNA-seq data obtained at the same growth phase as our phenotypic characterization experiments, illustrated in the outermost circle of Figure 1D [49]. Interestingly, 1D activity and 3D openness profiles show no correlation (Figure 1F), posing a puzzle and suggesting that the level of 3D interactions among chromosomal regions is largely unrelated (or minimally related) to their access to transcriptional resources. While one might anticipate a connection between openness, neighboring transcriptional activity, and circuit performance for inserted constructs, library results, as presented in the following sections, suggest there are no significant correlations. This indicates that general rules apply uniquely to the components of a circuit, and emphasizes the highly complex relationship between functional layers (i.e., DNA sequence and spatial location). Nevertheless, this chromosomal heterogeneity offers bioengineers diverse micro-environments to exploit. Figure 1F serves as a map to identify such locations, with orange spots indicating distinct dynamics in both interactions and transcription, as further highlighted in the complete circle (Figure 1F). Each location displays unique functional modulation benefits.

The positions of 191 space-specific transcriptional cascade circuits are depicted in Figure 1D, with one circular line per library. On each of these lines, inserts are indicated with a square, and the color intensity of each square reflects its performance represented as dynamic range normalized to that of the corresponding d=0 circuit inserted in the attTn7 site for a better comparison between libraries.

Evolution might already be leveraging space to optimize functions or develop entirely new ones. We compared the co-expressed genomic data of *P. putida* KT2440 against distance, considering both chromosomal distance (measured in base pairs) and three-dimensional physical distance (measured by HiC interaction strength) (Figure 1G). Results indicate that while most highly co-expressed genes are close together in genetic distance, with few co-expressed genes in distant genomic regions, when considering 3D distance the opposite trend is observed. Co-expressed genes are clearly clustered in three large groups, where the majority are located in regions that are separated in the 3D space. Although the discussion of these results is beyond the scope of this work, we believe that the natural utilization of space suggests that a synthetic application of the same is a tool we may want to exploit, as demonstrated next.

Re-programmable genetic switch

Out of the 221 engineered circuits, 30 were spatial variants of a genetic toggle switch (Figure 2A and Table S9). Importantly, the DNA sequence of the circuit remained unchanged

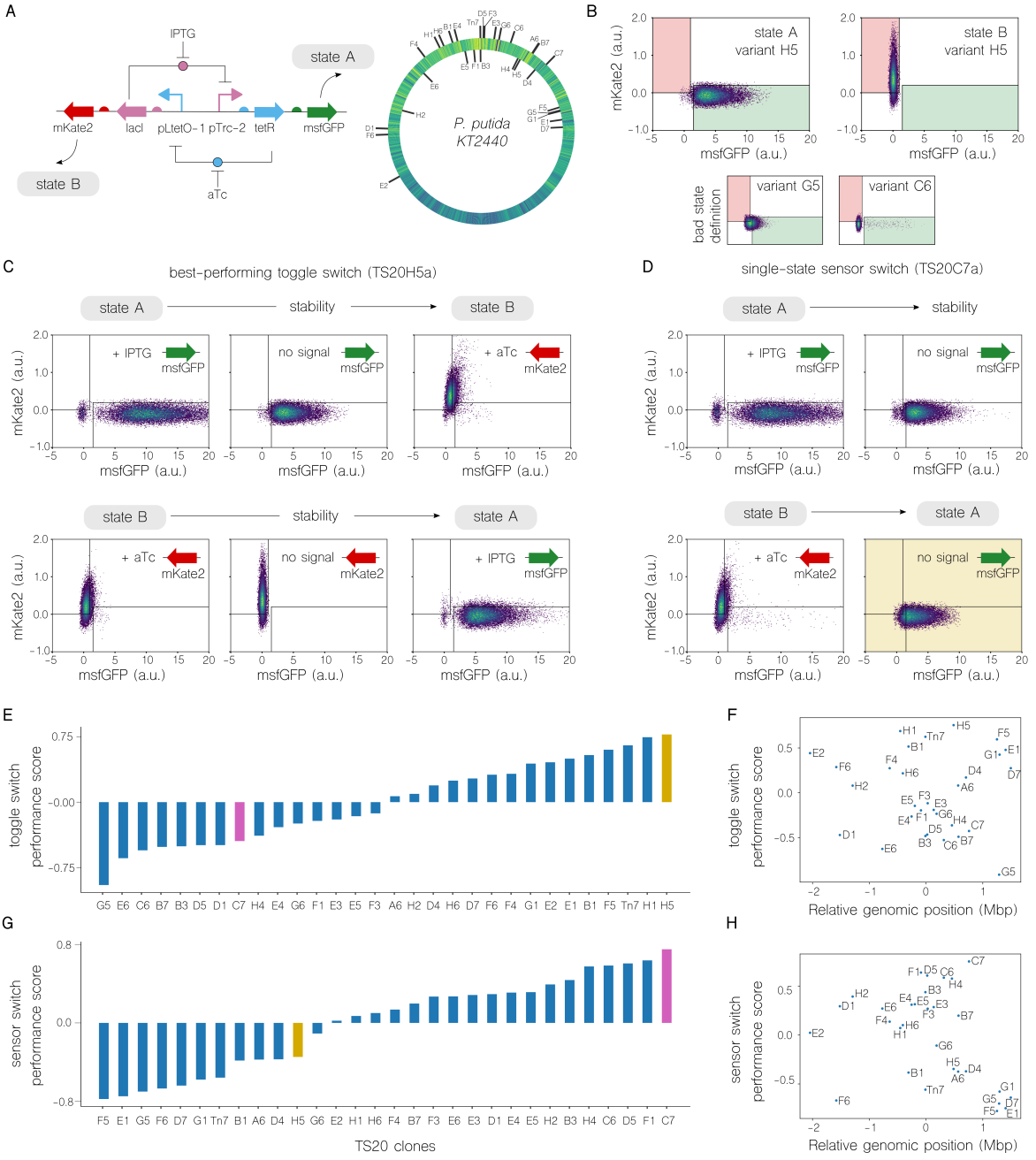

Figure 2: Re-programmable genetic switch. **A)** Schematic of the toggle switch (left). The genetic circuit comprising *tetR* and *lacI* genes, coding for repressor proteins TetR and LacI. These proteins suppress each other's expression, creating a toogle switch. Output is via mKate2 and msfGFP fluorescent proteins, regulated by TetR and LacI, respectively. The circuit transitions between states A and B with IPTG or aTc inducers. IPTG inactivates LacI, enabling *tetR* and msfGFP expression (state A), while aTc inactivates TetR, allowing *lacI* and mKate2 expression (state B). The right side of the panel illustrates the location of the 30 spatial variants of the genetic toggle switch within the Hi-C ring map of *P. putida* KT2440. (Continued on the following page.)

Figure 2: **B)** Density plots illustrating states A and B of the toggle switch for variant TS20H5a. The top-left plot demonstrates state A, with the cell population predominantly located within the green square. The top-right plot shows state B, where most cells fall within the red square. The two bottom plots present instances of suboptimal switching states for variants TS20G5a and TS20C6a, where the cell populations predominantly fall outside the designated squares, highlighting an undesirable or 'bad' state configuration. **C)** Performance of variant TS20H5a demonstrated through the transition dynamics between states A and B. The top row depicts the switch from state A to B, beginning with 4 hours of IPTG induction to achieve state A, followed by maintaining state A stability after IPTG removal for 20 hours, and concluding with a switch to state B after 4 hours of aTc induction. The bottom row reverses this process from state B to A. **D)** Performance of the variant TS20C7a as a sensor switch. The system maintains stability post-IPTG induction (top row), but loses stability and reverts to state A after aTc removal (bottom row), highlighting its differential response to inducers. **E)** and **G)** Performance scores of the 30 variants as toggle and sensor switches (see Methods for the score calculation). The best toggle switch variant, TS20H5a, performs poorly as a sensor switch, while the top sensor switch, TS20C7a, ranks low as a toggle switch. **F)** and **H)** Toggle and sensor switch performance scores relative to their genomic position. In both cases, toggles and sensors, the analysis reveals no significant correlations between the genomic positions and their performance.

across all variants, with the variations arising solely from differences in spatial positioning and the intrinsic constraints of specific locations. Given the constant DNA sequence, the toggle switches may be expected to display two states in all cases: either expressing green or red fluorescence. These states imply the activation of the circuit towards the msfGFP (state A) or mKate2 (state B) genes, respectively, while remaining inactive in the other direction. To induce these states, we used the same two signals: Isopropyl β- d-1-thiogalactopyranoside (IPTG) for turning on state A and anhydrotetracycline (aTc) for turning on state B. The definition and identifiability of the states is therefore the first basic fingerprint of this circuit. Notably, the stability of each state after removing the inducers represents the second fundamental feature of this bistable switch. The emphasis of this work is on the programmability of these two features by using spatial control.

Regarding the definition of states, we characterized circuits by assessing populations of each toggle switch variant after inducing with IPTG or aTc. This approach accounted for expression noise and intrinsic variability in both green and red fluorescent values. The states of the circuits were then evaluated based on population activity, aiming for clear distinctions between states without overlaps. In other words, when in state A, the activity of the population should be distinguishable from when the circuit was in state B. Figure 2B illustrates a well-defined separation, demonstrating that the area covered by cells expressing msfGFP (state A) does not overlap with the area covered by the same cells when expressing mKate2 (state B). The same figure also highlights instances of poorly-defined states, where a significant portion of the population expresses both genes simultaneously at different levels. This leads to circuits with suboptimal or even useless performance. Consequently, a toggle switch with poorly-defined states may possess a well-designed DNA sequence inadequately located within the chromosome. In such cases, altering the DNA parts is unnecessary; instead, relocating

the circuit to a different location is the key solution.

While reprogramming the definition of states could be used as an optimization strategy, reprogramming the stability of states can lead to the emergence of new functions. Within the library of 30 switches, some exhibit stability in one state but not in the other, while still preserving the ideal state definition. Stability refers to the ability to maintain a state once reached, regardless of whether the inducing signal that triggered the activation of that state is still present. A bistable switch, like the variant TS20H5a (Figure 2C), exemplifies this performance. After inducing with IPTG to activate state A, the signal can be removed, and the circuit retains the state permanently until the other inducing signal, aTc, turns off state A and triggers the activation of state B. Similarly, state B is also stable. In contrast, variant TS20C7a (Figure 2D) lacks stability in state B. Consequently, once in state B, the circuit autonomously transitions to reach state A as soon as aTc is removed, rendering it unstable. A potential mechanistic explanation for this behavior is that the strength of TetR and LacI (both in terms of expression and repression) is imbalanced, favoring the former over the latter. Even after removing aTc, TetR molecules manage to be expressed and quickly inhibit their target promoter. Such a monostable switch can be useful in scenarios where a default state is needed, and the other state will only be triggered temporarily while its sensing signal is present—function what we refer to as the sensor switch.

By classifying the 30 switch variants based on a good toggle switch performance (Figure 2E), we conclude that there is significant variability within the library with approximately 50% passing the quality test (see Methods). This means that the spatial location imposes key constraints on the functioning of the circuits. Interestingly, there is no correlation between switch performance and genomic position (Figure 2F). This strengthens the conclusion that spatial constraints are highly heterogeneous across chromosomal positions, with no general rules common to all. The advantage of this, from a biological design perspective, is that there may be as many microenvironments as positions, implying that space is a versatile modulation tool. Furthermore, our results suggest that poorly performing variants should not be discarded outright. For example, variant TS20C7, which shows poor toggle switch performance, functions very well as a sensor switch (Figure 2G), another possible scoring criterion that, again, has no correlation with genomic position (Figure 2H).

Phenotypic plasticity of transcriptional cascades inserted at different genomic positions

The phenotypic profiles of transcriptional cascades inserted at different genomic positions (Tables S3-S8) has been assessed by measuring the reporter's fluorescence upon induction with either IPTG, aTc or L-Arabinose at saturating concentrations. Flow cytometer measurements revealed different expression levels depending on the genomic location for all the transcriptional cascades (Figure 3A). Whereas variations in expression levels were to be expected based on previous studies [37, 38, 36], it is interesting to note the occurrence of non-standard distributions such as bimodal distribution (Figure 3A). Variations in expression and population distribution for a given variant were found at different genomic regions and chromosomal

strands. For example, the lowest fluorescent variant from the AraC libraries and the highest fluorescent variant from the LacI library have the transcriptional cascade inserted at close positions yet show opposite expression levels. Diving deeper into the performance of the transcriptional cascades we can observe that higher expression levels are not necessarily linked to better dynamic range. (Figure 3C). Previous research has proposed that insertion of synthetic circuits at rDNA yield higher expression and minimal interference with cellular fitness [33], however this does not guarantee a good circuit performance. In fact, library variants inserted at rDNA sites show a low dynamic range (low dynamic range AraC variants highlighted in Figure 3C). This emphasizes that the same genetic circuit at different genomic location can be modulated according to two variables: expression levels and dynamic range. This phenotypic variability appears to be a consequence of multiple variables since there is no correlation with the expression of upstream genes (Figure 3C), and it seems that gene dosage due to proximity to the origin of replication and proximity of the transcription factor to its cognate promoter in the 3D space are not the main causes of these differences (Figure 3D). The highest expression differences are observed for AraC libraries, whereas the highest variations in dynamic ranges are observed for the TetR library (Figure 3C). While both TetR and LacI are repressors, they show different patterns: LacI shows a lower dynamic range and expression level variation compared to TetR variants. Excepting AraC libraries, those where the transcription factor was spatially separated from its cognate promoter show similar expression levels to libraries were there is no separation (Figure 3B top). AraC is the only transcriptional activator that was integrated in this study and shows the highest differences when there is a physical distance between the transcription factor and its target promoter. As observed, all a_m variants show lower fluorescence on average than a_0 constructs where there is no distance. This is also evident in variants from both AraC libraries that have been inserted in the same genomic position (Figure 3E). However, it cannot be discarded that insertions in other locations could yield higher fluorescence. We observed differences in expression noise among the six transcriptional cascade libraries (Figure 3B bottom). In the activator library, noise levels in a_0 were lower compared to a_m. Interestingly, for the two repressors, we noticed an opposite trend. In the LacI library, noise appeared higher in l_m than in l_0. Conversely, in the TetR library, the noise in t_m was lower than in t_0. Another interesting observation is that insertions in position PP_5364 show opposite behaviours for AraC and TetR libraries depending on the distance of the transcription factor to its cognate promoter, lower fluorescence for a_m library and higher fluorescence for t_m (Figure 3E). Whether this is a result specific due to the different regulation mechanisms (AraC is an activator; TetR is a repressor) or particular to these transcription factor/promoter pairs remains to be determined.

Conclusions

This study highlights the pivotal role of spatial positioning on the functionality of synthetic genetic circuits in bacteria. By engineering 221 unique spatial configurations of genetic circuits, including toggle switches and regulatory cascades, this study demonstrates that the three-dimensional positioning of these circuits within a bacterial chromosome crucially affects

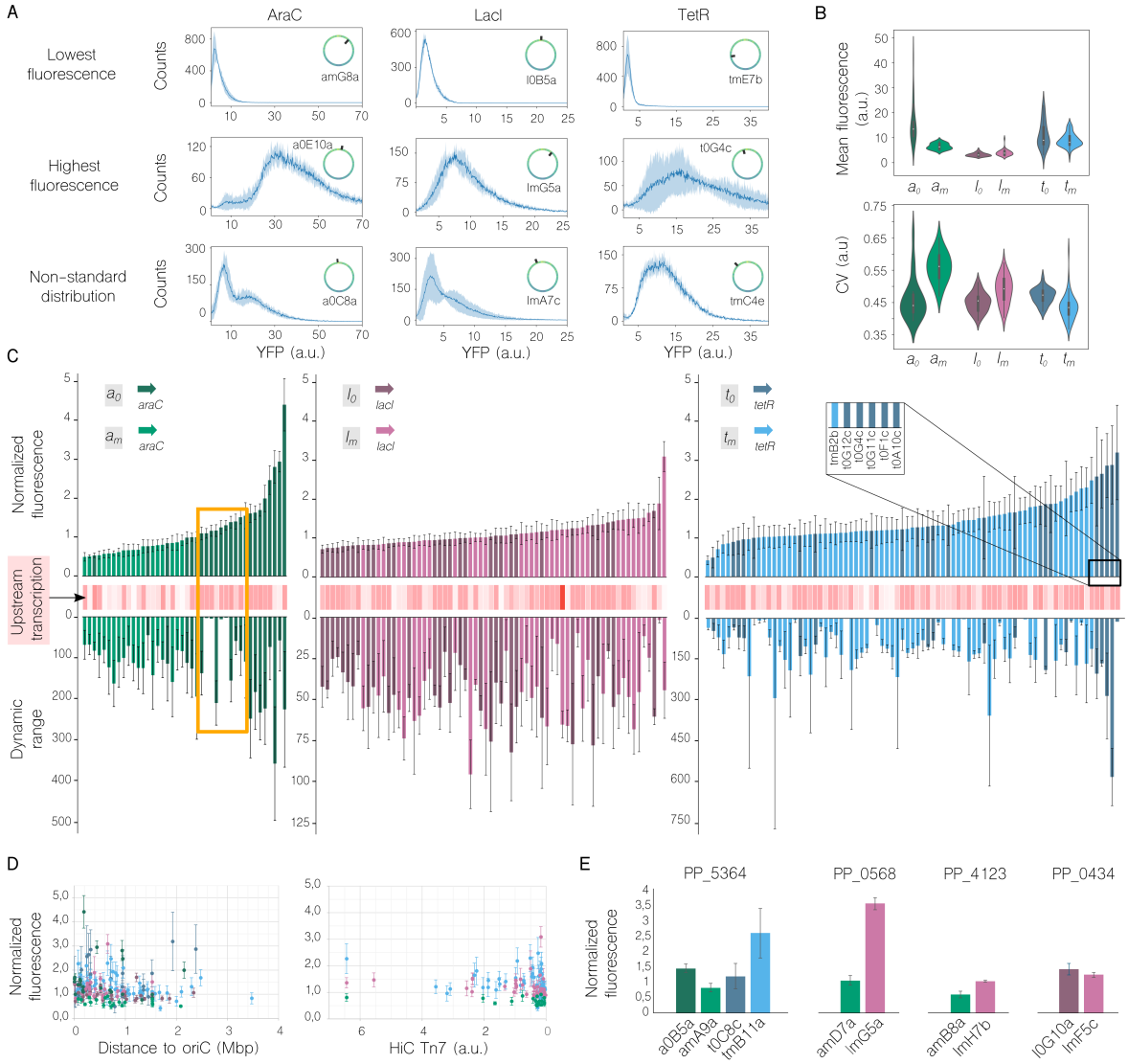

Figure 3: Transposon insertion libraries. **A)** Phenotypic variability in selected individual clones of AraC, LacI and TetR transcriptional cascade insertion libraries. **B)** Differences between AraC (a_0 = 23 clones; a_m = 19 clones), LacI (l_0 = 31 clones; l_m = 37 clones) and TetR (t_0 = 24 clones; t_m = 57 clones) libraries; mean fluorescence (top) and coefficient of variation (bottom). **C)** Phenotypic characterization of individual clones. Normalized fluorescence to the corresponding transcriptional cascade inserted at attTn7 for each library (top), transcription of upstream gene for each inserted variant (middle) and dynamic range (bottom). Insertion libraries are ordered as AraC (left), LacI (middle) and TetR (right). **D)** Normalized fluorescence for each library against distance to oriC (left) and Hi-C interactions, with respect to attTn7 site, for a_m, t_m and l_m libraries (right). **E)** Fluorescence comparison between variants inserted at the same position.

their performance. Key findings include the ability to reprogram circuits for different outputs by altering their chromosomal locations, revealing that spatial arrangement can optimize circuit functionality and introduce new operational modes. We used space to reprogram the stability of circuit states, turning toggle switches into sensor switches, and to precisely control gene expression noise patterns, ranging from full expression to bimodal activity and beyond.

This research underscores the importance of considering three-dimensional space in genetic circuit design, moving beyond traditional linear component arrangements, and offers foundational insights for leveraging intracellular space as a design parameter.

3 Material and Methods

Strains, media and general culture conditions

LB media was used to culture both *E. coli* and *P. putida* strains except when M9 minimal media supplemented with 0.2% (v/w) citrate was required: during certain steps of the conjugation protocol according to previous references ([50]; [51]) and for the cultivation of library clones for flow cytometry. Antibiotics were used at the following concentrations: kanamycin (Km) 50 µg/mL, chloramphenicol (Cm) 50 µg/mL, gentamicin (Gm) 10 µg/mL, and ampicillin (Ap) 150 µg/mL for *E. coli*, while 500 µg/mL for *P. putida*. *E. coli* and *P. putida* strains were cultured at 37^{o}C and 30^{o}C respectively. For every specific library, inducers were added at the following concentrations: Isopropyl β-D-1-thiogalactopyranoside (IPTG) 2 mM, anhydrotetracyclin (aTc) 50 ng/µL, and L-arabinose (L-ara) 1% . The list of strains used in this work is shown in Table 1. *P. putida* KT2440 was the receiver strain for every integration event. A set of *E. coli* strains coding for pir protein were used as parental strains in order to keep suicide vectors (pBAMD1.2, pBLAM1.2 and pTn7-M derivatives built in this study; Table 2). *E. coli*HB101 bearing pRK600 was used as the helper strain for all integrations, while *E. coli* DH5$\alpha\lambda$pir transformed with pTNS2 plasmid (carrying a transposase) assisted mini-Tn7 transpositions.

Strain	Genotype	Source
Escherichia coli pir2	F- δ(argF-lac)169 rpoS(Am) robA1 creC510 hsdR514 endA recA1 uidA(δMluI)::pir+	Invitrogen
Escherichia coli DH5$\alpha\lambda$pir	F-, supE44, δlacU169, (φ80 lacZDM15), hsdR17, (rkmk+), recA1, endA1, thi1, gyrA, relA, pir+, π+	[50] [52]
Escherichia coli HB101	F–, thi-1, hsdS20 (rB–, mB–), supE44, recA13, ara-14, leuB6, proA2, lacY1, galK2, rpsL20 (strR), xyl-5, mtl-1.	[53]
Pseudomonas putida KT2440	Prototrophic, wild-type strain derived of P. putida mt-2 without pWW0 plasmid	[46]

Table 1: List of strains used in this study

DNA assemblies

Plasmids used and built in this study are listed in Table 2. Genetic circuit sequences aTc-TetR-pTet, IPTG-LacI-pTac, 3MB-XylS-pM, Lara-AraC-pBAD were ordered from Doulix (Rome, Italy) and Toggle Switch Class 2 (TS2) fragments TS2-TetR-msfGFP and TS2-LacI-mKate2 from Twist Bioscience (California, USA). TS2 fragments were assembled to generate the toggle switch circuit via a touchdown SOE-PCR protocol from [54]. DNA was cloned using either classical restriction and ligation ([55]; restriction enzymes, T4 DNA ligase and Quick Ligation kit from New England Biolabs, Ipswich, Massachusetts, USA) or isothermal assembly ([56]; Gibson Assembly MasterMix, New England Biolabs, Ipswich, Massachusetts, USA). Plasmid pBLAM1-2-TS2-msfGFP-mKate2 was subjected whole-plasmid site-directed mutagenesis[57] to eliminate MmeI site in the TetR gene. DNA oligos (Table S2) were ordered to IDT (Coralville, Iowa, USA) and polymerase enzymes used for DNA amplification were Phusion (Thermo Fisher Scientific, Waltham, Massachusetts, USA) or Q5 (New England Biolabs, Ipswich, Massachusetts, USA). The construction method for each plasmid built in this work can be consulted in Table S1. Minipreps were performed using Monarch Plasmid Miniprep kit (New England Biolabs, Ipswich, Massachusetts, USA) and PCR products were purified with Monarch PCR and DNA Cleanup kit (New England Biolabs, Ipswich, Massachusetts, USA).

Construction, selection, and genotyping of transposon insertion libraries

Once pTn7-M, pBAMD1.2 and pBLAM1.2 derivative suicide plasmids were built, they were delivered into *P. putida* KT2440 chromosome following a conjugation protocol previously described for transpositions into gram-negative bacteria [50] [51]). Conjugation outcome was processed in order to separate variants, discard spurious integrations and genotype the transposon location in accordance with an automated high-throughput screening method [63] using LAP protocols [64]. Selected and genotyped libraries were stored at -80^{o}C for further phenotypic characterization. The genomic location of the inserted genetic circuits separated by library can be consulted in Tables S3-S9.

Flow cytometry

96-well flat-bottomed plates were filled with 100 µL of LB per well plus the proper antibiotic and inoculated with selected variants previously stored at -80^{o}C. This preinoculum was placed at 30^{o}C with shaking for an O/N incubation. The following day, 1 µL of the preinoculum was used to inoculate a new plate filled with 100 µL of filtered M9 media supplemented with 0.2% (v/w) citrate plus the proper antibiotic and the corresponding inducer at saturating concentrations (2 mM IPTG, 1% L-Arabinose or 100 ng/µL aTc). This plate was incubated at 30^{o}C with 500 rpm shaking for 4 hours. After that incubation time, well content was diluted with 150 µL M9 citrate in order to dilute cultures and balance the events per second required for an adequate flow cytometry measurement. For Toggle switch variants, after 4h induction with either 100 ng/µL aTc, 2 mM IPTG or not inductor, 20 µL were diluted with

Plasmid	Description	Reference
pRK600	tra+, mob+, CmR, oriV ColE1, helper plasmid transformed into *E. coli* HB101 to assist conjugation between donor and receiver strain.	[58]
pTNS2	TnsABCD specific transposition pathway, ApR, OriV R6K, transposase plasmid transformed into *E. coli* DH5$\alpha\lambda$pir to assist conjugation between mini-Tn7 donnor and receiver strain	[59]
pBAMD1.2	Mini-Tn5 delivery plasmid tnpA+, ME-I and ME-O extremes, oriV R6K, ApR KmR	[60]
pBLAM1.2	MarC9 transposase, IR-I and IR-O extremes, oriV R6K, ApR KmR	[61]
pTn7-M	Tn7L and Tn7R extremes, OriV R6K, GmR KmR	[62]
pTn7-LacI	pTn7 derivative, lacI repressor	This work (GenBank PP480516)
pTn7-IPTG-LacI-pTac-YFP	pTn7 derivative, lacI repressor, YFP controlled under pTac promoter	This work (GenBank PP480518)
pTn7-TetR	pTn7 derivative, tetR repressor	This work (GenBank PP480512)
pTn7-aTc-TetR-pTet-YFP	pTn7 derivative, tetR repressor, YFP controlled under pTet promoter	This work (GenBank PP480513)
pTn7-AraC	pTn7 derivative, araC regulator	This work (GenBank PP480508)
pTn7-Lara-AraC-pBAD-YFP	pTn7 derivative, araC regulator, YFP controlled under pBAD promoter	This work (GenBank PP480509)
pTn7-TS2-msfGFP-mKate2	pTn7 derivative, toggle switch: LacI regulator, mKate2 controlled under pTet promoter and TetR regulator, msfGFP controlled under pTrc promoter	This work (GenBank PP489398)
pBLAM1.2-TS2-msfGFP-mKate2	pBLAM1.2 derivative, toggle switch: LacI regulator, mKate2 controlled under pTet promoter and TetR regulator, msfGFP controlled under pTrc promoter	This work (GenBank PP489399)
pBAMD1.2-pTac-YFP	pBAMD1.2 derivative, YFP controlled under pTac promoter	This work (GenBank PP480517)
pBAMD1.2-IPTG-LacI-pTac-YFP	pBAMD1.2 derivative, lacI repressor, YFP controlled under pTac promoter	This work (GenBank PP480515)
pBLAM1.2-IPTG-LacI-pTac-YFP	pLAMD1.2 derivative, lacI repressor, YFP controlled under pTac promoter	This work (GenBank PP480519)
pBAMD1.2-pTet-YFP	pBAMD1.2 derivative, YFP controlled under pTet promoter	This work (GenBank PP480511)
pBAMD1.2-aTc-TetR-pTet-YFP	pBAMD1.2 derivative, tetR repressor, YFP controlled under pTet promoter	This work (GenBank PP480514)
pBLAM1.2-aTc-TetR-pTet-YFP	pBLAM1.2 derivative, tetR repressor, YFP controlled under pTet promoter	This work (GenBank PP489397)
pBAMD1.2-pBAD-YFP	pBAMD1.2 derivative, YFP controlled under pBAD promoter	This work (GenBank PP480507)
pBAMD1.2-Lara-AraC-pBAD-YFP	pBAMD1.2 derivative, araC regulator, YFP controlled under pBAD promoter	This work (GenBank PP480506)
pBLAM1.2-Lara-AraC-pBAD-YFP	pBLAM1.2 derivative, araC regulator, YFP controlled under pBAD promoter	This work (GenBank PP480510)

Table 2: List of plasmids used in this work

100 µL M9 citrate and measured in the flow cytometer; the remaining 80 µL of culture were diluted in 800 µL of M9 citrate, centrifuged at 2204 × g and resuspended in 100 µL of M9 citrate to wash chemical inductors. Toggle switch cultures were grown at 30^{o}C with shaking for 20h without inductors, 10 µL of cultures were diluted with 100 µL of M9 citrate and measured in the flow cytometer and 1 µL used to inoculate 100 µL of M9 citrate with the

opposite inducer (IPTG for variants previously induced with aTc or aTc for those induced with IPTG) or no inductor. After 4h of growth at 30ºC with shaking, cultures were measured in the flow cytometer. Cultures were passed through a MACSQuant VYB Flow Cytometer (Miltenyi Biotec, Germany) at a maximum speed of 20,000 events per second up to 100,000 singlet events. All variants were measured at least in triplicate. To clean the cytometry raw data, we applied several gates to each sample. Outliers were removed across all channels using the z-score parameter. Next, gating was applied to the FSC-A and SSC-A density plots, and doublets were eliminated using gating on the SSC-H versus SSC-A density plot. After data cleaning, 20,000 events from each sample were randomly selected for the final analysis.

RNAseq data analysis

RNASeq raw data of replicates of *P.putida* KT2440 in exponential phase grown in M9-citrate liquid media were obtained from [49]. To calculate transcription expression levels, data was processed using Geneious prime 2023.2.1 (Biomatters Ltd, New Zealand). Reads were aligned to the reference genome of *P.putida* KT2440 (Accession number NC_002947.3) using the built-in Geneious RNA mapper. Transcripts per million (TPM) for reads mapped against the annotated reference genome were calculated using the built-in function "Calculate expression levels".

HiC data acquisition and analysis

P.putida KT2440 and *P.putida* KT-GFP strains were grown overnight from a glycerol stock at 30ºC with shaking. These precultures were inoculated into 5 mL M9-citrate at OD600nm of 0.1 and grown at 30ºC for 4h. Cultures were then centrifuged, fixed with formaldehyde following Phase Genomics (Seattle, Washington, USA) guidelines and sent for HiC processing (DNA extraction, digestion with Sau3AI and MluCI restriction enzymes and sequencing). HiC reads QC analysis was performed by Phase Genomics. Each culture was sent in duplicate. Analysis of HiC reads in .fastq format was performed using the TADbit software pipeline, built as a Singularity image from a modified specification that is made publicly available on github. The pipeline used is as follows:

1. Index the reference genome using gem3-mapper.
2. Map reads to the reference genome using gem3-mapper.
3. Parse and filter reads using the default filters employed by the TADbit filter tool.
4. Assign filtered reads into bins of 5000bp
5. Normalise bins using the "Vanilla" normalisation offered by TADbit (single iteration ICE normalisation).
6. Convert bin list to matrix format.

More details of the analysis can be obtained by inspecting the script we used to run the pipeline, which is publicly available on github and contains the specific arguments given to TADbit for each step.

Score calculation

For the calculation of the toggle switch performance, we used the following equations:

$$S^t_{total} = S^t_A S^t_B - \langle S^t_A S^t_B \rangle \tag{1}$$

$$S^t_A = \frac{1}{n_I} \sum_{i=1}^{n_I} f_i^I + \frac{1}{n_{I_r}} \sum_{i=1}^{n_{I_r}} f_i^{I_r} \tag{2}$$

$$S^t_B = \frac{1}{n_a} \sum_{i=1}^{n_a} f_i^a + \frac{1}{n_{a_r}} \sum_{i=1}^{n_{ar}} f_i^{a_r}, \tag{3}$$

where S^t_{total} is the total performance score, S^t_A and S^t_B are the scores for states A and B, respectively. f_i^I and $f_i^{I_r}$ represent the fraction of events in the green square after IPTG induction and removal, while f_i^a and $f_i^{a_r}$ denote the fraction in the red square after aTc induction and removal, respectively. n_I and n_a are the numbers of replicates for IPTG and aTc inductions, while n_{I_r} and n_{a_r} are the numbers of replicates after IPTG and aTc removal, respectively.

For the calculation of the sensor switch performance, we used the following equations:

$$S^s_{total} = S^s_A S^s_B - \langle S^s_A S^s_B \rangle \tag{4}$$

$$S^s_A = \frac{1}{m_I} \sum_{i=1}^{m_I} g_i^I + \frac{1}{m_{I_r}} \sum_{i=1}^{m_{I_r}} g_i^{I_r} + \frac{1}{m_{a_r}} \sum_{i=1}^{m_{a_r}} g_i^{a_r} \tag{5}$$

$$S^s_B = \frac{1}{m_a} \sum_{i=1}^{m_a} g_i^a, \tag{6}$$

where S^s_{total} is the total performance score, S^s_A and S^s_B are the scores for states A and B, respectively. g_i^I, $g_i^{I_r}$, $g_i^{a_r}$ represent the fraction of events in the green square after IPTG induction, IPTG removal, and aTC removal, respectively. g_i^a denotes the fraction in the red square after aTc induction. m_I and m_a are the numbers of replicates for IPTG and aTc inductions, while m_{I_r} and n_{a_r} are the numbers of replicates after IPTG and aTc removal, respectively.

All experiments involving the toggle library were conducted in quadruplicate. Only samples that passed the flow cytometry gating criteria were considered for the score calculation.

References

[1] Y. Benenson, "Biomolecular computing systems: principles, progress and potential," *Nature Reviews Genetics*, vol. 13, no. 7, pp. 455–468, 2012.

[2] E. Andrianantoandro, S. Basu, D. K. Karig, and R. Weiss, "Synthetic biology: new engineering rules for an emerging discipline," *Molecular systems biology*, vol. 2, no. 1, pp. 2006–0028, 2006.

[3] M. Amos and A. Goñi-Moreno, "Cellular computing and synthetic biology," *Computational matter*, pp. 93–110, 2018.

[4] L. Grozinger, M. Amos, T. E. Gorochowski, P. Carbonell, D. A. Oyarzún, R. Stoof, H. Fellermann, P. Zuliani, H. Tas, and A. Goñi-Moreno, "Pathways to cellular supremacy in biocomputing," *Nature communications*, vol. 10, no. 1, p. 5250, 2019.

[5] V. Chubukov, A. Mukhopadhyay, C. J. Petzold, J. D. Keasling, and H. G. Martín, "Synthetic and systems biology for microbial production of commodity chemicals," *NPJ systems biology and applications*, vol. 2, no. 1, pp. 1–11, 2016.

[6] V. De Lorenzo, K. L. Prather, G.-Q. Chen, E. O'Day, C. von Kameke, D. A. Oyarzún, L. Hosta-Rigau, H. Alsafar, C. Cao, W. Ji, *et al.*, "The power of synthetic biology for bioproduction, remediation and pollution control: the un's sustainable development goals will inevitably require the application of molecular biology and biotechnology on a global scale," *EMBO reports*, vol. 19, no. 4, p. e45658, 2018.

[7] S. Slomovic, K. Pardee, and J. J. Collins, "Synthetic biology devices for in vitro and in vivo diagnostics," *Proceedings of the National Academy of Sciences*, vol. 112, no. 47, pp. 14429–14435, 2015.

[8] A. A. Nielsen, B. S. Der, J. Shin, P. Vaidyanathan, V. Paralanov, E. A. Strychalski, D. Ross, D. Densmore, and C. A. Voigt, "Genetic circuit design automation," *Science*, vol. 352, no. 6281, p. aac7341, 2016.

[9] M. W. Gander, J. D. Vrana, W. E. Voje, J. M. Carothers, and E. Klavins, "Digital logic circuits in yeast with crispr-dcas9 nor gates," *Nature communications*, vol. 8, no. 1, p. 15459, 2017.

[10] T. K. Kassaw, A. J. Donayre-Torres, M. S. Antunes, K. J. Morey, and J. I. Medford, "Engineering synthetic regulatory circuits in plants," *Plant Science*, vol. 273, pp. 13–22, 2018.

[11] M. Mansouri and M. Fussenegger, "Therapeutic cell engineering: designing programmable synthetic genetic circuits in mammalian cells," *Protein & Cell*, vol. 13, no. 7, pp. 476–489, 2022.

[12] B. A. Blount, T. Weenink, S. Vasylechko, and T. Ellis, "Rational diversification of a promoter providing fine-tuned expression and orthogonal regulation for synthetic biology," *PloS one*, vol. 7, no. 3, p. e33279, 2012.

[13] R. G. Egbert and E. Klavins, "Fine-tuning gene networks using simple sequence repeats," *Proceedings of the National Academy of Sciences*, vol. 109, no. 42, pp. 16817–16822, 2012.

[14] A. Boo, T. Ellis, and G.-B. Stan, "Host-aware synthetic biology," *Current Opinion in Systems Biology*, vol. 14, pp. 66–72, 2019.

[15] C. Moschner, C. Wedd, and S. Bakshi, "The context matrix: Navigating biological complexity for advanced biodesign," *Frontiers in Bioengineering and Biotechnology*, vol. 10, 2022.

[16] S. A. Scholz, C. D. Lindeboom, and P. L. Freddolino, "Genetic context effects can override canonical cis regulatory elements in Escherichia coli," *Nucleic Acids Research*, vol. 50, pp. 10360–10375, Oct. 2022.

[17] H. Tas, L. Grozinger, R. Stoof, V. de Lorenzo, and Á. Goñi-Moreno, "Contextual dependencies expand the re-usability of genetic inverters," *Nature communications*, vol. 12, no. 1, p. 355, 2021.

[18] I. V. Surovtsev and C. Jacobs-Wagner, "Subcellular organization: a critical feature of bacterial cell replication," *Cell*, vol. 172, no. 6, pp. 1271–1293, 2018.

[19] J. Kim, A. Goñi-Moreno, and V. de Lorenzo, "Subcellular architecture of the xyl gene expression flow of the tol catabolic plasmid of pseudomonas putida mt-2," *mBio*, vol. 12, no. 1, pp. 10–1128, 2021.

[20] A. Soler-Bistué, M. Timmermans, and D. Mazel, "The Proximity of Ribosomal Protein Genes to oriC Enhances Vibrio cholerae Fitness in the Absence of Multifork Replication," *mBio*, vol. 8, pp. e.00097–17, Feb. 2017.

[21] E. Garmendia, G. Brandis, and D. Hughes, "Transcriptional Regulation Buffers Gene Dosage Effects on a Highly Expressed Operon in Salmonella," *mBio*, vol. 9, pp. e01446–18, Sept. 2018.

[22] J. Fan, H. El Sayyed, O. J. Pambos, M. Stracy, J. Kyropoulos, and A. N. Kapanidis, "RNA polymerase redistribution supports growth in E. coli strains with a minimal number of rRNA operons," *Nucleic Acids Research*, vol. 51, pp. 8085–8101, Aug. 2023.

[23] M. M. Babu, S. C. Janga, I. de Santiago, and A. Pombo, "Eukaryotic gene regulation in three dimensions and its impact on genome evolution," *Current opinion in genetics & development*, vol. 18, no. 6, pp. 571–582, 2008.

[24] S. Leidescher, J. Ribisel, S. Ullrich, Y. Feodorova, E. Hildebrand, A. Galitsyna, S. Bultmann, S. Link, K. Thanisch, C. Mulholland, *et al.*, "Spatial organization of transcribed eukaryotic genes," *Nature cell biology*, vol. 24, no. 3, pp. 327–339, 2022.

[25] D. B. Brückner, H. Chen, L. Barinov, B. Zoller, and T. Gregor, "Stochastic motion and transcriptional dynamics of pairs of distal DNA loci on a compacted chromosome," *Science*, vol. 380, pp. 1357–1362, 2023.

[26] M. Campos and C. Jacobs-Wagner, "Cellular organization of the transfer of genetic information," *Current Opinion in Microbiology*, vol. 16, pp. 171–176, Apr. 2013.

[27] M. Irastortza-Olaziregi and O. Amster-Choder, "Coupled Transcription-Translation in Prokaryotes: An Old Couple With New Surprises," *Frontiers in Microbiology*, vol. 11, p. 624830, Jan. 2021.

[28] J. Kim, A. Goñi-Moreno, B. Calles, and V. de Lorenzo, "Spatial organization of the gene expression hardware in Pseudomonas putida," *Environmental Microbiology*, vol. 21, no. 5, pp. 1645–1658, 2019. Section: 1645.

[29] S. A. Scholz, R. Diao, M. B. Wolfe, E. M. Fivenson, X. N. Lin, and P. L. Freddolino, "High-Resolution Mapping of the Escherichia coli Chromosome Reveals Positions of High and Low Transcription," *Cell Systems*, vol. 8, pp. 212–225.e9, Mar. 2019.

[30] K. M. Dahlstrom and G. A. O'Toole, "A Symphony of Cyclases: Specificity in Diguanylate Cyclase Signaling," *Annu Rev Microbiol*, vol. 71, pp. 179–195, Sept. 2017.

[31] T. E. Saleski, M. T. Chung, D. N. Carruthers, A. Khasbaatar, K. Kurabayashi, and X. N. Lin, "Optimized gene expression from bacterial chromosome by high-throughput integration and screening," *Science Advances*, vol. 7, p. eabe1767, Feb. 2021.

[32] A. Hueso-Gil, B. Calles, and V. de Lorenzo, "In Vivo Sampling of Intracellular Heterogeneity of Pseudomonas putida Enables Multiobjective Optimization of Genetic Devices," *ACS Synthetic Biology*, May 2023.

[33] A. Domröse, J. Hage-Hülsmann, S. Thies, R. Weihmann, L. Kruse, M. Otto, N. Wierckx, K.-E. Jaeger, T. Drepper, and A. Loeschcke, "Pseudomonas putida rDNA is a favored site for the expression of biosynthetic genes," *Scientific Reports*, vol. 9, p. 7028, Dec. 2019.

[34] J. E. Chaves, R. Wilton, Y. Gao, N. M. Munoz, M. C. Burnet, Z. Schmitz, J. Rowan, L. H. Burdick, J. Elmore, A. Guss, D. Close, J. K. Magnuson, K. E. Burnum-Johnson, and J. K. Michener, "Evaluation of chromosomal insertion loci in the Pseudomonas putida KT2440 genome for predictable biosystems design," *Metabolic Engineering Communications*, vol. 11, p. e00139, Dec. 2020.

[35] M. Wolański, R. Donczew, A. Zawilak-Pawlik, and J. Zakrzewska-Czerwińska, "oriC-encoded instructions for the initiation of bacterial chromosome replication," *Frontiers in Microbiology*, vol. 5, 2015.

[36] D. H. S. Block, R. Hussein, L. W. Liang, and H. N. Lim, "Regulatory consequences of gene translocation in bacteria," *Nucleic Acids Research*, vol. 40, no. 18, pp. 8979–8992, 2012. Section: 8979.

[37] T. E. Kuhlman and E. C. Cox, "Gene location and dna density determine transcription factor distributions in *Escherichia coli*," *Molecular Systems Biology*, vol. 8, no. 1, p. 610, 2012.

[38] J. A. Bryant, L. E. Sellars, S. J. W. Busby, and D. J. Lee, "Chromosome position effects on gene expression in Escherichia coli K-12," *Nucleic Acids Research*, vol. 42, pp. 11383–11392, 09 2014.

[39] V. Gerganova, M. Berger, E. Zaldastanishvili, P. Sobetzko, C. Lafon, M. Mourez, A. Travers, and G. Muskhelishvili, "Chromosomal position shift of a regulatory gene alters the bacterial phenotype," *Nucleic Acids Research*, vol. 43, pp. 8215–8226, Sept. 2015.

[40] Á. Goñi-Moreno, I. Benedetti, J. Kim, and V. de Lorenzo, "Deconvolution of gene expression noise into spatial dynamics of transcription factor–promoter interplay," *ACS synthetic biology*, vol. 6, no. 7, pp. 1359–1369, 2017.

[41] Y. Park, A. Espah Borujeni, T. E. Gorochowski, J. Shin, and C. A. Voigt, "P recision design of stable genetic circuits carried in highly-insulated e. coli genomic landing pads," *Molecular systems biology*, vol. 16, no. 8, p. e9584, 2020.

[42] R. T. Dame, F.-Z. M. Rashid, and D. C. Grainger, "Chromosome organization in bacteria: mechanistic insights into genome structure and function," *Nature Reviews Genetics*, vol. 21, pp. 227–242, Apr. 2020.

[43] Z. Li, H. Yang, Y. Wang, S.-H. Chou, and J. He, "The spatial position effect: synthetic biology enters the era of 3D genomics," *Trends in Biotechnology*, vol. 40, pp. 539–548, 2022.

[44] E. Yeung, A. J. Dy, K. B. Martin, A. H. Ng, D. Del Vecchio, J. L. Beck, J. J. Collins, and R. M. Murray, "Biophysical constraints arising from compositional context in synthetic gene networks," *Cell Systems*, vol. 5, no. 1, pp. 11–24.e12, 2017.

[45] E. Martínez-García and V. de Lorenzo, "Pseudomonas putida as a synthetic biology chassis and a metabolic engineering platform," *Current Opinion in Biotechnology*, vol. 85, p. 103025, 2024.

[46] K. E. Nelson, C. Weinel, I. T. Paulsen, R. J. Dodson, H. Hilbert, V. a. P. Martins dos Santos, D. E. Fouts, S. R. Gill, M. Pop, M. Holmes, L. Brinkac, M. Beanan, R. T. DeBoy, S. Daugherty, J. Kolonay, R. Madupu, W. Nelson, O. White, J. Peterson, H. Khouri, I. Hance, P. C. Lee, E. Holtzapple, D. Scanlan, K. Tran, A. Moazzez, T. Utterback, M. Rizzo, K. Lee, D. Kosack, D. Moestl, H. Wedler, J. Lauber, D. Stjepandic, J. Hoheisel, M. Straetz, S. Heim, C. Kiewitz, J. Eisen, K. N. Timmis, A. Düsterhöft, B. Tümmler, and C. M. Fraser, "Complete genome sequence and comparative analysis of the metabolically versatile Pseudomonas putida KT2440," *Environmental Microbiology*, vol. 4, no. 12, pp. 799–808, 2002.

[47] H. Tas, L. Grozinger, A. Goñi-Moreno, and V. de Lorenzo, "Automated design and implementation of a nor gate in pseudomonas putida," *Synthetic Biology*, vol. 6, no. 1, p. ysab024, 2021.

[48] H. Tas, Á. Goñi-Moreno, and V. d. Lorenzo, "A standardized inverter package borne by broad host range plasmids for genetic circuit design in gram-negative bacteria," *ACS synthetic biology*, vol. 10, no. 1, pp. 213–217, 2020.

[49] Hueso-Gil, B. Calles, G. A. O'Toole, and V. De Lorenzo, "Gross transcriptomic analysis of *Pseudomonas putida* for diagnosing environmental shifts," *Microbial Biotechnology*, vol. 13, pp. 263–273, Jan. 2020.

[50] E. Martínez-García, B. Calles, M. Arévalo-Rodríguez, and V. de Lorenzo, "pBAM1: an all-synthetic genetic tool for analysis and construction of complex bacterial phenotypes," *BMC Microbiology*, vol. 11, p. 38, Feb. 2011.

[51] E. Martínez-García and V. de Lorenzo, "Engineering multiple genomic deletions in Gram-negative bacteria: analysis of the multi-resistant antibiotic profile of Pseudomonas putida KT2440," *Environmental Microbiology*, vol. 13, no. 10, pp. 2702–2716, 2011.

[52] D. Hanahan, "Studies on transformation of Escherichia coli with plasmids," *Journal of Molecular Biology*, vol. 166, pp. 557–580, June 1983.

[53] J. J. Schmidt, "DNA cloning: A practical approach," *Biochemical Education*, vol. 14, no. 2, pp. 190–245, 1986.

[54] R. S. Hilgarth and T. M. Lanigan, "Optimization of overlap extension PCR for efficient transgene construction," *MethodsX*, vol. 7, p. 100759, Jan. 2020.

[55] J. Sambrook, E. F. Fritsch, and T. Maniatis, *Molecular Cloning: A Laboratory Manual*. Cold Spring Harbor Laboratory, 1989.

[56] D. G. Gibson, L. Young, R.-Y. Chuang, J. C. Venter, C. A. Hutchison, and H. O. Smith, "Enzymatic assembly of DNA molecules up to several hundred kilobases," *Nat Methods*, vol. 6, pp. 343–345, May 2009.

[57] M. Laible and K. Boonrod, "Homemade site directed mutagenesis of whole plasmids," *J Vis Exp*, May 2009.

[58] B. Kessler, V. de Lorenzo, and K. N. Timmis, "A general system to integrate lacZ fusions into the chromosomes of gram-negative eubacteria: regulation of the Pm promoter of the TOL plasmid studied with all controlling elements in monocopy," *Mol Gen Genet*, vol. 233, pp. 293–301, May 1992.

[59] K.-H. Choi, J. B. Gaynor, K. G. White, C. Lopez, C. M. Bosio, R. R. Karkhoff-Schweizer, and H. P. Schweizer, "A Tn7-based broad-range bacterial cloning and expression system," *Nat Methods*, vol. 2, pp. 443–448, June 2005.

[60] E. Martínez-García, T. Aparicio, V. de Lorenzo, and P. I. Nikel, "New Transposon Tools Tailored for Metabolic Engineering of Gram-Negative Microbial Cell Factories," *Frontiers in Bioengineering and Biotechnology*, vol. 2, 2014.

[61] L. Alejaldre, A.-M. Anhel, and Goñi-Moreno, "pBLAM1-x: standardized transposon tools for high-throughput screening," *Synthetic Biology*, vol. 8, no. 1, p. ysad012, 2023.

[62] S. Zobel, I. Benedetti, L. Eisenbach, V. de Lorenzo, N. Wierckx, and L. M. Blank, "Tn7-Based Device for Calibrated Heterologous Gene Expression in Pseudomonas putida," *ACS Synthetic Biology*, vol. 4, no. 12, pp. 1341–1351, 2015.

[63] L. Alejaldre, A. M. Anhel, and Goñi-Moreno, "High-throughput workflow for the genotypic characterization of transposon library variants," *protocols.io:dx.doi.org/10.17504/protocols.io.kqdg394jzg25/v1*, Oct. 2022.

[64] A.-M. Anhel, L. Alejaldre, and Á. Goñi-Moreno, "The laboratory automation protocol (lap) format and repository: a platform for enhancing workflow efficiency in synthetic biology," *ACS synthetic biology*, vol. 12, no. 12, pp. 3514–3520, 2023.

Acknowledgments

This work was supported by the grants BioSinT-CM (Y2020/TCS-6555) and CONTEXT (Atracción de Talento Program; 2019-T1/BIO-14053) Projects of the Comunidad de Madrid, MULTI-SYSBIO (PID2020-117205GA-I00) funded by MICIU/AEI/ 10.13039/501100011033, and the ECCO (ERC-2021-COG-101044360) Contract of the EU.